Check for updates

Received: 3 September 2021 | Revised: 7 November 2021 | Accepted: 13 December 2021

DOI: 10.1002/jbm.a.37348

RESEARCH ARTICLE

Society For Biomaterials | WILEY

Investigation of creep properties and the cytoskeletal structures of non-tumorigenic breast cells and triple-negative breast cancer cells

Killian Onwudiwe[1] | John Obayemi[2,3] | Jingjie Hu[4,5] | Josephine Oparah[1] | Chinyerem Onyekanne[1] | Chukwudalu Nwazojie[1] | Toyin Aina[1] | Vanessa Uzonwanne[3] | Ali Salifu[2] | Winston Soboyejo[1,2,3]

[1]Department of Materials Science and Engineering, Biomaterials Lab, African University of Science and Technology, Abuja, Nigeria

[2]Department of Biomedical Engineering, Gateway Park Life Sciences Center, Worcester Polytechnic Institute (WPI), Worcester, Massachusetts, USA

[3]Department of Mechanical and Materials Engineering, Worcester Polytechnic Institute (WPI), Worcester, Massachusetts, USA

[4]Division of Vascular and Interventional Radiology, Mayo Clinic, Scottsdale, Arizona, USA

[5]Department of Mechanical and Aerospace Engineering, North Carolina State University, Raleigh, North Carolina, USA

Correspondence
Winston Soboyejo, Boynton Hall, Worcester Polytechnic Institute, 100 Institute Road, Worcester, MA 01609, USA.
Email: wsoboyejo@wpi.edu

Funding information
This research was supported by the Pan African Materials Institute (PAMI) with a grant from the African Centers of Excellence (ACE) Program (Grant No. P126974) that was funded by the World Bank.

Abstract

This article presents the correlation of creep and viscoelastic properties to the cytoskeletal structure of both tumorigenic and non-tumorigenic cells. Unique shear assay and strain mapping techniques were used to study the creep and viscoelastic properties of single non-tumorigenic and tumorigenic cells. At least 20 individual cells, three locations per cell, were studied. From the results, lower densities in the volume of actin, and keratin 18 structures were observed with the progression of cancer and were correlated to the increased creep rates and reduced mechanical properties (Young's moduli and viscosities) of tumorigenic (MDA-MB-231) cells. The study reveals significant differences between the creep and viscoelastic properties of non-tumorigenic breast cells versus tumorigenic cells. The variations in the creep strain rates are shown to be well characterized by lognormal distributions, while the statistical variations in the viscoelastic properties are well-described by normal distributions. The implications of the results are discussed for the study of discrete cell behaviors, strain and viscoelastic responses of the cell, and the role of cell cytoskeleton in the onset and progression of cancers.

KEYWORDS
cancer detection, cell viscoelastic/creep properties, confocal microscopy, cytoskeletal proteins, immunofluorescence staining, relative volume density, shear assay

1 | INTRODUCTION

In the last few decades, there has been an increased emphasis on the diagnosis and treatment of difficult-to-treat diseases such as cancer, which is one of the leading causes of death globally.[1,2] Breast cancer, on the other hand, has been recorded as the most diagnosed cancer in women and constitutes the highest rate of mortality by cancer in women worldwide, second in Africa, and fifth in the west pacific.[3–5] Triple-negative breast cancer (TNBC), which is prevalent in most women of African descent, tests negative for estrogen receptor, progesterone receptor, and human epidermal growth factor receptor-2,[6–9] and therefore poses a more imminent threat to these women in Africa, owing to its difficult prognosis and clinical outcomes.[10,11] Therefore, there is a strong need for a more targeted diagnostic technique and treatment pathway, to help combat the challenges posed by this type of cancer.

To address the challenges in cancer diagnosis, recent studies have demonstrated the role of cell mechanics in the characterization of cells into benign, less metastatic, c, and highly metastatic cells, using different mechanical techniques.[12–22] It was observed that in most

15524965, 2022, 5, Downloaded from https://onlinelibrary.wiley.com/doi/10.1002/jbm.a.37348 by Tsinghua University Library, Wiley Online Library on [05/11/2022]. See the Terms and Conditions (https://onlinelibrary.wiley.com/terms-and-conditions) on Wiley Online Library for rules of use; OA articles are governed by the applicable Creative Commons License

cases, normal cells had relatively higher mechanical properties compared to cancerous cells.[23–26] The variations in the mechanical properties of the cells were, however, linked to the different compositions of the cell cytoskeletal structures at varying stages of cancer progression.[13,25,27–31] The cytoskeletal structure of the cell (Figure 1) is a heterogeneous structure that consists of different cell proteins, the actin filaments, microtubules, and intermediate filament,[32–35] and it is primarily responsible for structural support, localization, and transport of organelles in the cell, and intracellular trafficking.[23,25] The cell cytoskeleton plays an important role in the study of the mechanical properties of the cell, and in the development of mechanical biomarkers for the detection of diseases such as cancer, a disease characterized by marked tumor heterogeneity and diverse molecular orientations.[25,36,37] Figure 1A,B show the schematic of the cytoskeletal structures of a cell and the stained images for the different protein structures of the cell cytoskeleton respectively. In Figure 1B, the staining of the actin cytoskeletal proteins and the nucleus are shown in red and blue, while the intermediate filaments and microtubules are shown in green. Prior research has also shown that the overexpression of some cytoskeletal proteins can provide indicators of tumor progression.[37]

In a prior work by our research group, we studied the viscoelastic properties of non-tumorigenic breast cells and tumorigenic TNBC cells and their relationship with actin cytoskeletal structure.[24,25] The mechanical properties of the cell were seen to reduce relatively with cancer progression, and the fluorescence intensities of actin filaments

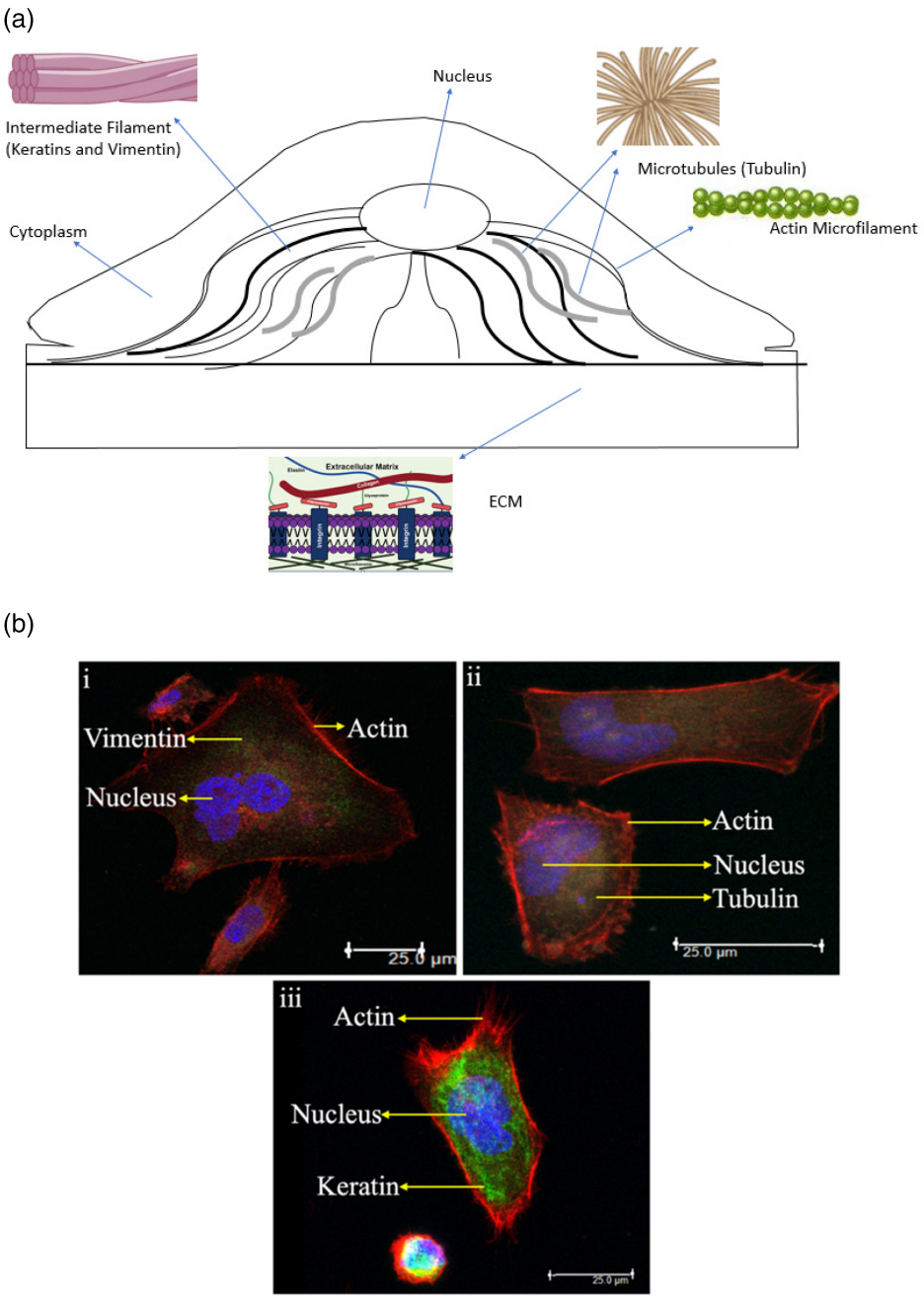


FIGURE 1 (A) Stained images showing the different protein structures of the cell cytoskeleton (Figure insets adapted https://courses.lumenlearning.com/sanjacinto-biology1/chapter/the-cytoskeleton/). (B) Schematic of cytoskeletal structures in a biological cell

15524965, 2022, 5, Downloaded from https://onlinelibrary.wiley.com/doi/10.1002/jbm.a.37348 by Tsinghua University Library, Wiley Online Library on [05/11/2022]. See the Terms and Conditions (https://onlinelibrary.wiley.com/terms-and-conditions) on Wiley Online Library for rules of use; OA articles are governed by the applicable Creative Commons License

in the breast cells were found to decrease with increasing metastasis of breast cancer.[23–25] The reduction in the actin filament of the cell cytoskeleton was, however, correlated with the reduction in cell stiffness.[24]

However, the role of creep in cell deformation studies and the contributions of the other components of the cytoskeletal structure (keratin 7, 8, 18, and 19; vimentin, and microtubules such as tubulin) have not been considered in our prior work.

In this study, local variations in the viscoelastic and creep properties of the cell were studied using the shear assay technique and strain mapping techniques with digital image correlation (DIC) software, which can distinguish between the local properties of the cells at different regions within the cell. The variations in the strain rates and strain evolution of the cells are good indicators of the contributions of the cell proteins/structure to the deformation and mechanical properties of the cell. The effects of the cell cytoskeleton on the spatial variations of cell creep and viscoelastic properties were also studied. The implications of the current work are discussed for the study of discrete cell behaviors, strain and viscoelastic responses of the cell, and the role of cell cytoskeleton in the onset and progression of cancers.

2 | MATERIALS AND METHODS

2.1 | Cell culture

The normal breast cell (MCF-10A) and the metastatic breast cell (MDA-MB-231) were cultured under conditions described previously in a study by Reference 23. The cells were cultured in 60 × 15 × 35 mm falcon Petri dishes (Corning Inc., Corning, NY) for a duration of 48 h. This was done at 37°C in 5% CO_2, at atmospheric pressure, to allow adequate time for the attachment and growth of the cells on the substrate. Under these conditions, the MCF-10A cells were grown using Dulbecco's modified eagle medium (DMEM)/Ham's F-12 medium (Invitrogen, Carlsbad, CA) at an equal mix ratio of 1:1, together with a supplemented 5% horse serum (Invitrogen, Carlsbad, CA), 0.2% amphotericin (Gemini Bio-Products, West Sacramento, CA), 30 ng/ml insulin (Sigma-Aldrich, St. Louis, MO), 100 ng/ml cholera toxin (Sigma Aldrich), 30 ng/ml murine epidermal growth factor (Peprotech), 0.5 g/ml hydrocortisone (Sigma Aldrich) and 1% Penicillin Streptomycin (Invitrogen, Carlsbad, CA). On the other hand, the MDA-MB-231 cells were grown at the same conditions in a 10% fetal bovine serum from the American Type Culture Collection (ATCC) (Manassas, VA) and in an L-15 base media, with a supplemented 100 I.U/ml penicillin/100 μg/ml streptomycin respectively.

2.2 | Immunofluorescence cell staining

The cytoskeletal structures of the different cells MCF-10A and MDA-MB-231 were stained to reveal the distribution and relative volume density of the different cytoskeletal proteins (actin, Keratin, vimentin, and tubulin). Each cell was stained to reveal: the nucleus; actin filaments; intermediate filaments, and microtubules (tubulin). The staining protocols are the same as summarized in our previous work.[23] A 4% high-grade paraformaldehyde (4% in 0.1 PBS, Electron Microscopy Science, Hatfield, PA) was used to fixate the cells after culturing for 48 h. This was followed by the aspiration of the paraformaldehyde and rinsing thoroughly with a phosphate buffer solution (PBS) diluted with deionized water. The cells were each permeabilized for 10 min with 1 ml of 0.1% Triton X-100 solution (Life Technologies Corporation, Carlsbad, CA).

Furthermore, the cells were then incubated in PBS with 1% of bovine serum albumin (BSA) (Sigma-Aldrich, St. Louis, MO) at room temperature (25°C) for 1 h, after which they were rinsed thoroughly with PBS. Staining for any of the cell proteins was done using the protein's specific antibody. For keratin 7, 8, 18, and 19, cytokeratin 7, 8, 18, and 19 mouse monoclonal antibody at 2 μg/ml in 0.1% BSA was used. Tubulin alpha rabbit polyclonal antibody (Thermo Fisher Scientific) at 2 μg/ml in 0.1% BSA was used for the tubulin staining, and lastly, for vimentin, vimentin mouse monoclonal antibody (Thermo Fisher Scientific, Waltham, MA) was used at 2 μg/ml in 0.1% BSA. The labeled proteins were incubated for 3 h at room temperature (25°C), before rinsing with PBS. The cells were then further labeled with Goat anti-Mouse IgG (H+L) superclonal™ secondary antibody Alexa Fluor® 488 conjugate (Thermo Fisher Scientific, Waltham, MA) at a dilution of 1:2000, after which the cells were further rinsed properly in PBS and incubated in a dark environment for 25 min, at room temperature. The resulting structures were further stained in PBS with F-actin stain Rhodamine Phalloidin (Thermo Fisher Scientific, Waltham, MA), followed by proper rinsing with PBS.

The MCF-10A and MDA-MB-231 cells were subcultured on coverslips and fixed with 4% (v/v) paraformaldehyde for 15 min and at room temperature. A mixture of diluted water and Dulbecco's phosphate-buffered saline (DPBS) was used to wash the cells three times. The cells were blocked using 1%(w/v) pharmingen Stain Buffer (BSA) prepared with PBS for 15 min at room temperature. The samples were then rehydrated in PBS for 10 min and washed again with DiH_20+DPBS.

The resulting cells were then stained simultaneously with Alexa-488 phalloidin (A12379) and Alexa-594 DnaSe1-deoxyribonuclease 1, Alexa flour™ 594 conjugates (D12372) (Invitrogen, USA) for staining F-actin and G-actin, respectively. This was done by adding 200 μl of a 9 μg/ml solution of fluorescent DNase 1in a buffer to the coverslip. I unit (200 μl of a 0.165 μM solution) of fluorescent phallotoxin was used to simultaneously label F-actin, for 20 min. The cells were washed with DiH_20+DPBS. The nuclei of the cells were stained using SlowFade® Gold Antifade Mountant with DAPI (Thermo Fisher Scientific, Waltham, MA) for 2 min. The samples were mounted on a clean glass slide in a medium of Fluoro Guard Reagent drop. The imaging of the stained cell samples was done using a ×60 oil immersion objective, and an inverted Leica SP5 point Scanning Confocal Microscope (Leica Microsystems, Heidelberg, Germany). Leica LAS AF Lite software was used to determine the total intensity per given area for the tubulin, keratins, actin, and vimentin.

15524965, 2022, 5, Downloaded from https://onlinelibrary.wiley.com/doi/10.1002/jbm.a.37348 by Tsinghua University Library, Wiley Online Library on [05/11/2022]. See the Terms and Conditions (https://onlinelibrary.wiley.com/terms-and-conditions) on Wiley Online Library for rules of use; OA articles are governed by the applicable Creative Commons License

2.3 | Confocal imaging and analysis

The stained cells were imaged under a confocal microscope (an inverted Leica SP5 point scanning confocal microscope, Leica microsystems, Heidelberg, Germany) using a ×40 oil immersion objective. The actin cytoskeleton was imaged with a wavelength of 565 nm excitation, while the other intermediate filaments (vimentin, keratin 19, keratin 18, keratin 8, keratin 7) and microtubulin, were imaged with a wavelength of 488 nm excitation. The nucleus was also imaged with a wavelength of 488 nm excitation. The cells were imaged under identical system parameter settings, at a z-stack height of 1 μm, and an average of 20–30 slices per cell. The fluorescence intensities (intensity per unit area) of the proteins of each cell line were estimated using the three-dimensional confocal image stacks. However, the variation in intensities for the individual proteins of the normal cell was compared with that of the cancer cells. The image visualization and analysis were carried out using the Leica software. The total amount of fluorescence was measured according to the protocol reported in a previous study.[38,39]

2.4 | Shear assay experiments

The shear assay experiment was used in this study to exert mechanical forces in the form of fluid pressure to biological cells (MCF-10A and MDA-MB-231), and hence the mechanical response of these cells to an applied force was subsequently observed.[40] This, however, translates to the further determination of the cell viscoelastic properties of the non-tumorigenic and tumorigenic breast cells using other mechanical techniques such as strain mapping and the use of viscoelastic models. An average of 20 single cells per cell line was sampled for this study. Figure 2 below shows the experimental setup involved in the determination of the mechanical response of the cells as a function of the external forces. The cells were cultured in a Petri dish (35 × 10 mm) (CELL TREAT scientific products, MA) as shown in Figure 2B. The process further involves the fitting of the microfluidic device chamber, together with the rubber gasket in between. This setup is connected to the syringe pump with the help of tubing, and then placed on the optical microscope for imaging and monitoring. The programmable syringe pump (Figure 2A), then infuses and withdraws the fluid medium through the use of syringes and tubing and is kept at a constant flow rate (3 ml/min), ensuring a continuous flow of fluid over the surface of the cell. This controlled flow of fluid is carried out within a microfluidic flow chamber as shown in Figure 2C, fitted unto the Petri dish with the help of the rubber gasket (Figure 2D), which helps ensure controlled fluid flow between the microfluidic device and the Petri dish. The rubber gasket is circular, with tiny holes, and serves as a vacuum suction. It has a rectangular channel in the middle (20.5 mm—length, 2.5 mm—width, and 0.254 mm—height) that determines the flow profile. The controlled flow of fluid within the parallel flow chamber generates the desirable wall shear stresses. The process of shearing-off of the cells and determining how the fluid flow affects the mechanical and structural integrity of the cells is captured

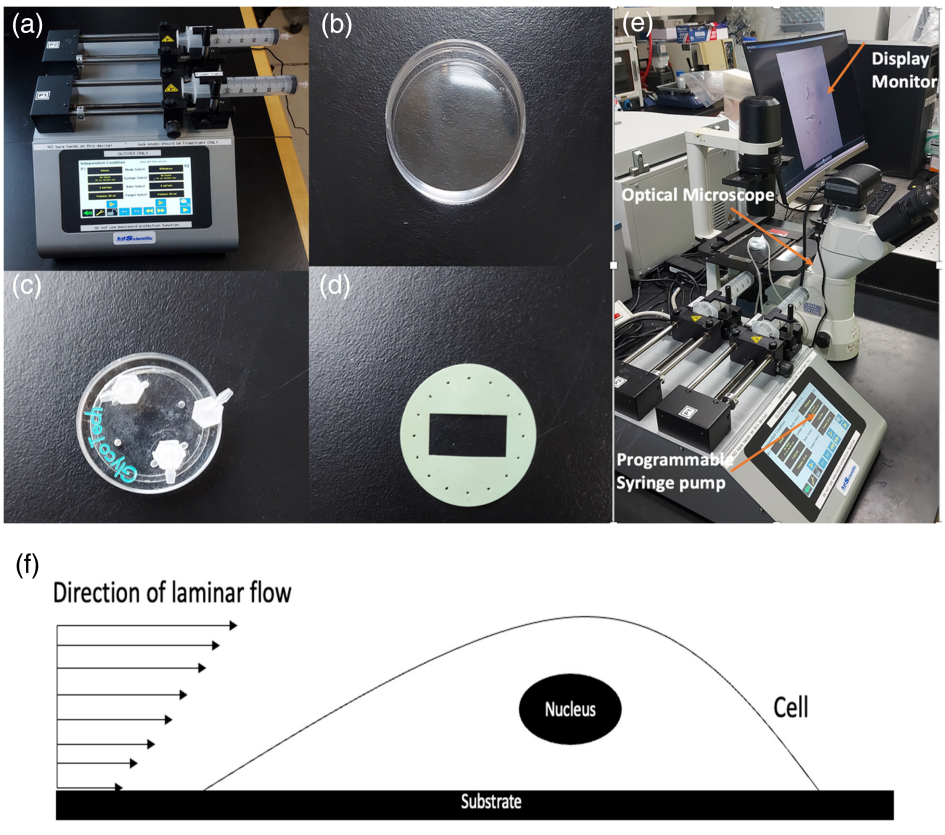


FIGURE 2 (A) Programmable syringe pump (B) 35 × 10 mm Petri dish for cell culture (C) microfluidic flow chamber (D) rubber gasket (E) complete experimental set-up (F) schematic of laminar flow over cell

15524965, 2022, 5, Downloaded from https://onlinelibrary.wiley.com/doi/10.1002/jbm.a.37348 by Tsinghua University Library, Wiley Online Library on [05/11/2022]. See the Terms and Conditions (https://onlinelibrary.wiley.com/terms-and-conditions) on Wiley Online Library for rules of use; OA articles are governed by the applicable Creative Commons License

by the optical microscope and displayed on a computer monitor as shown in Figure 2E.

Formula for the determination of the wall shear stress is given as

$$\sigma = \frac{6\mu Q}{wh^2,} \quad (1)$$

where is σ is the wall shear stress, μ is the viscosity of the fluid medium, Q is the flow rate, W is the width of the channel (rubber gasket), and H is the height of the channel (rubber gasket).

To prevent nonspecific binding of the extracellular matrix protein, a serum-free culture media was used for cell culture. In most cases, methylcellulose which is nontoxic and nonallergenic is added to the serum-free media to increase the viscosity of the cell culture medium. This is the case in MCF-10A cells, where 3.5 wt% methylcellulose is added to the culture media to obtain a viscosity of 0.16 Pa s. For the MDA-Mb-231 cells, no cellulose was added, and hence the viscosity of the media was 0.02 Pa s. This is because less shear stress is

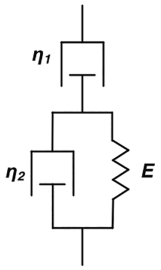


FIGURE 3 Schematic of the three-element generalized Maxwell model

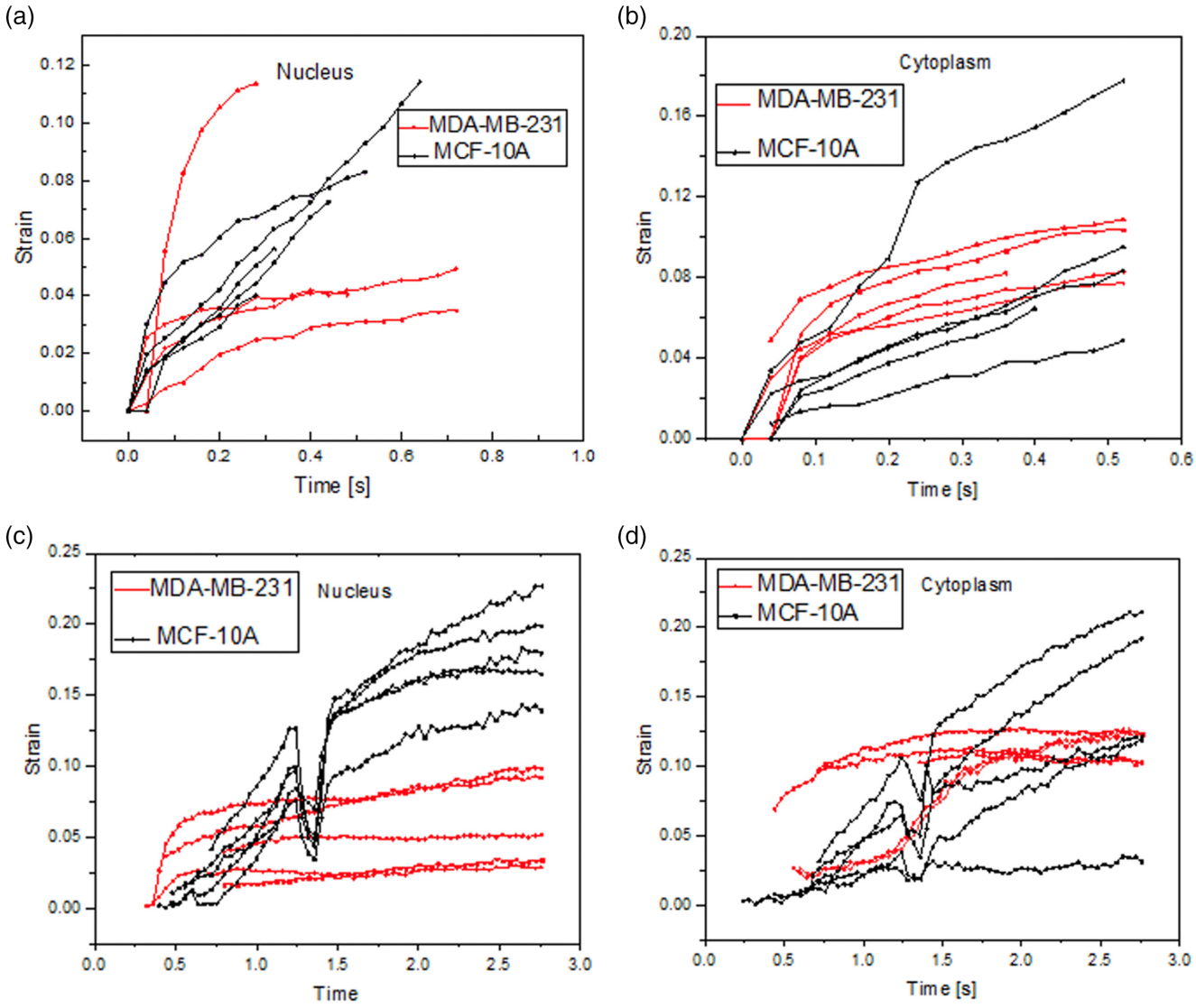


FIGURE 4 A five-data plot representative of (A) single-cell strain evolution for the nucleus of the cells at the primary (elastic) creep stage. (B) Single-cell strain evolution for the cytoplasm of the cells at the primary (elastic) creep stage. (C) Single-cell evolution for the nucleus of the cells at the secondary creep stage. (D) Single-cell evolution for the cytoplasm of the cells at the secondary creep stage

15524965, 2022, 5, Downloaded from https://onlinelibrary.wiley.com/doi/10.1002/jbm.a.37348 by Tsinghua University Library, Wiley Online Library on [05/11/2022]. See the Terms and Conditions (https://onlinelibrary.wiley.com/terms-and-conditions) on Wiley Online Library for rules of use; OA articles are governed by the applicable Creative Commons License

required to deform or shear off the MDA-MB-231 cells. However, the shear rates for both the MCF-10A and MDA-MB-231 cells are similar (2500 s^{-1}), and the wall shear stress for the shearing-off of MCF-10A and MDA-MB-231 was 410 and 10 Pa, respectively. The Reynolds number was ensured to be within the laminar flow regime (Re < 100).

To ensure that the same fluid temperature is maintained and delivered to the cells, and to avoid disturbance of the cells during the experiments, the flow medium was pre-heated to 37°C in a water bath, and residual bubbles in the flow line were evacuated by pre-flushing the tubing alongside the medium. The cells were subjected to controlled shear stresses by keeping the flow and velocities uniform. The response of the cells to shear stresses was observed in situ using an optical microscope and a video camera. The movements and detachment of isolated single cells from their substrates without the interference of the adjacent neighboring cells were monitored using the ×40 objective lens from Nikon. The detachment/dislocation of the cells (nucleus and cytoplasm) were recorded and stopped when the cells detached from the substrate. The individual frames from the recordings were extracted for the DIC analysis. This technique proves to be a potential mechanical means for cell characterization, and is proposed for the characterization of cells into their component cell states.

2.5 | Strain mapping

To determine the mechanical behavior of these cells (MCF-10A and MDA-MB-231), their deformation images obtained during the shear assay experiment were analyzed using the DIC software. The changes in the cell structure (nucleus and cytoplasm) were tracked by locating each pixel block in the images of the deformed cell structure. From the images of the cell as obtained during the shear assay experiment, a position in the nucleus and cytoplasm of the cell is marked and tracked to determine the magnitude of strain experienced during deformation. As the cell deforms, the displacement of the cell with respect to time is determined as the position of the cell structure changes during deformation from the marked position to a new position. For an optimized correlation value, a subset size of 31 × 31 pixels and a step size of eight pixels were chosen. The step size defines the difference in the distance of the subset before the next correlation.

2.6 | Viscoelastic modeling

The viscoelastic properties of the cell define the cell as both viscous and elastic material. In our study, the cells were subjected to constant stress and thus experienced creep. The creep region was, however, analyzed using the three-element generalized Maxwell model as shown in Figure 3. This model describes a time-dependent strain due to viscoelastic effects and can be defined by Equation (2), which shows the relationship between the various parameters.

$$\varepsilon = \left(\frac{\sigma}{\eta 1}\right)t + \frac{\sigma}{E}\left(1 - \exp\left(-\frac{t}{\tau}\right)\right). \quad (2)$$

The viscous behavior is accounted by the top dashpot and is thus represented by $\left(\frac{\sigma}{\eta 1}\right)t$. The combination of the spring and dashpot in parallel represents the Voigt model. The spring component on the right of the model represents the elasticity of the material. The effective viscosity of the cell is obtained by the top dashpot value $\eta 1$, and the relaxation time (τ) is given by the ratio of the elasticity and the viscosity of the dashpot $\eta 2$, in the Voigt component, and hence it is given as $\frac{\eta 2}{E}$.

The viscoelastic properties of the cell were thus determined by using the equation for the viscoelastic model as shown in Equation (2)

TABLE 1 Statistical analysis for strain evolution of the cells at the onset of deformation (primary creep regime)

Cells	Av. strain (nucleus)	Av. strain (cytoplasm)	Tukey's sig value[a]	FPC mean grouping (nucleus)[b]	FPC mean grouping (cytoplasm)[b]
MCF-10A	0.08406	0.12409	1	A	B
MDA-MB-231	0.01977	0.03425	1	B	A

[a]Means with Tukey's sig value =1, is significantly different.
[b]Means that do not share a letter are significantly different (Fisher pairwise comparisons [FPC]).

TABLE 2 Statistical analysis for strain evolution of the cells at complete deformation

Cells	Av. strain (nucleus)	Av. strain (cytoplasm)	Tukey's sig value[a]	FPC mean grouping (nucleus)[b]	FPC mean grouping (cytoplasm)[b]
MCF-10A	0.13634	0.20844	1	A	A
MDA-MB-231	0.03613	0.07377	1	B	B

[a]Means with Tukey's sig value =1, is significantly different.
[b]Means that do not share a letter are significantly different (Fisher pairwise comparisons [FPC]).

15524965, 2022, 5, Downloaded from https://onlinelibrary.wiley.com/doi/10.1002/jbm.a.37348 by Tsinghua University Library, Wiley Online Library on [05/11/2022]. See the Terms and Conditions (https://onlinelibrary.wiley.com/terms-and-conditions) on Wiley Online Library for rules of use; OA articles are governed by the applicable Creative Commons License

to fit the strain-time data with the curve fitting tool in MATLAB. The fitting parameters $\left(\frac{\sigma}{\eta 1}, \frac{\sigma}{E}, \frac{E}{\eta 2}\right)$ were adjusted to yield high R^2. The viscoelastic properties, therefore, were extracted from the fitting parameters. From the parameters, ε represents the strain, σ represents the wall shear stress, E represents the elastic modulus, $\eta 1$ represents the viscosity, and τ represents the relaxation time.

2.7 | Statistical analysis

The statistical analyses of the creep properties and the fluorescence intensities of the different cytoskeleton proteins of the non-tumorigenic and tumorigenic TNBC cells were carried out using the Minitab 18 software package (Minitab LLC, State College, PA). For each cytoskeletal protein, the statistical variations of the fluorescence intensities were determined for the two cell types (MCF-10A and MDA-MB-231) using a one-way analysis of variance (ANOVA) and Fisher pairwise comparisons. The ANOVA was done for equal variances at a confidence level of 95%, and a significance level of 0.05 that was adopted for the analysis.

For the ANOVA, the null hypothesis (H_0) assumes equal means between the different cell types of the proteins, suggesting that the variation between the cell types (MC-10A and MDA-MB-231) was insignificant, and therefore the p-value must be >.05. The alternative hypothesis (H_a) assumes that the means of the different cell types are not equal, which suggests that there are significant differences between the mean properties of the different cells, and as such the p-values must be <.05. Furthermore, the similarities and variations in their intensities were established using the frequency distribution curves.

3 | RESULTS

3.1 | Single-cell strain mapping and strain evolution

The single-cell images of the different types of cells were analyzed using the DIC machine, and hence, the differences in the strain evolution between the nucleus and the cytoplasm of different cell types

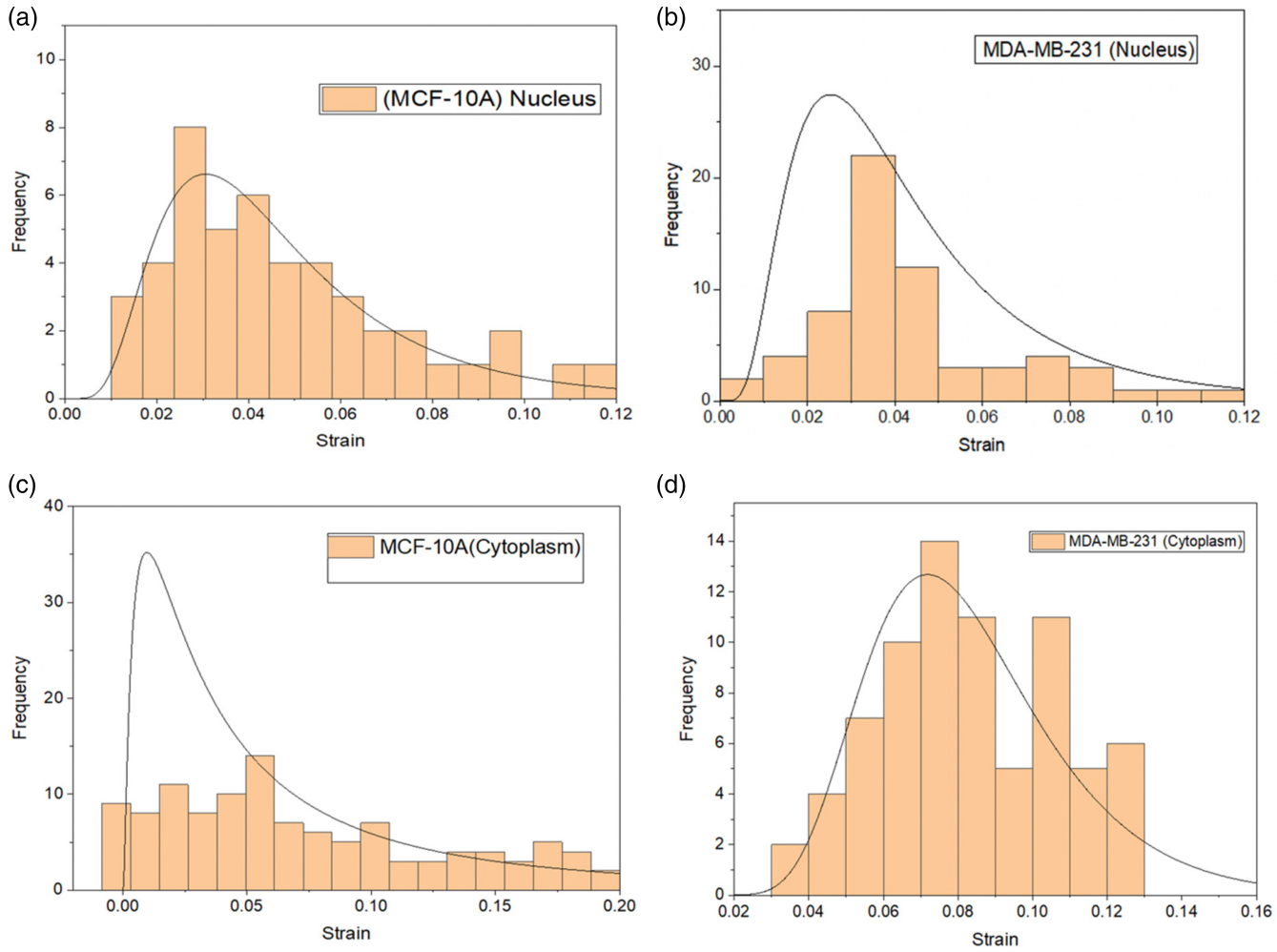


FIGURE 5 Frequency distribution at the onset of creep (Primary creep), for (A) the nucleus of the MCF-10A cell, (B) the nucleus of the MDA-MB-231, (C) cytoplasm of the MCF-10A, and (D) the cytoplasm of the MDA-MB-231

15524965, 2022, 5, Downloaded from https://onlinelibrary.wiley.com/doi/10.1002/jbm.a.37348 by Tsinghua University Library, Wiley Online Library on [05/11/2022]. See the Terms and Conditions (https://onlinelibrary.wiley.com/terms-and-conditions) on Wiley Online Library for rules of use; OA articles are governed by the applicable Creative Commons License

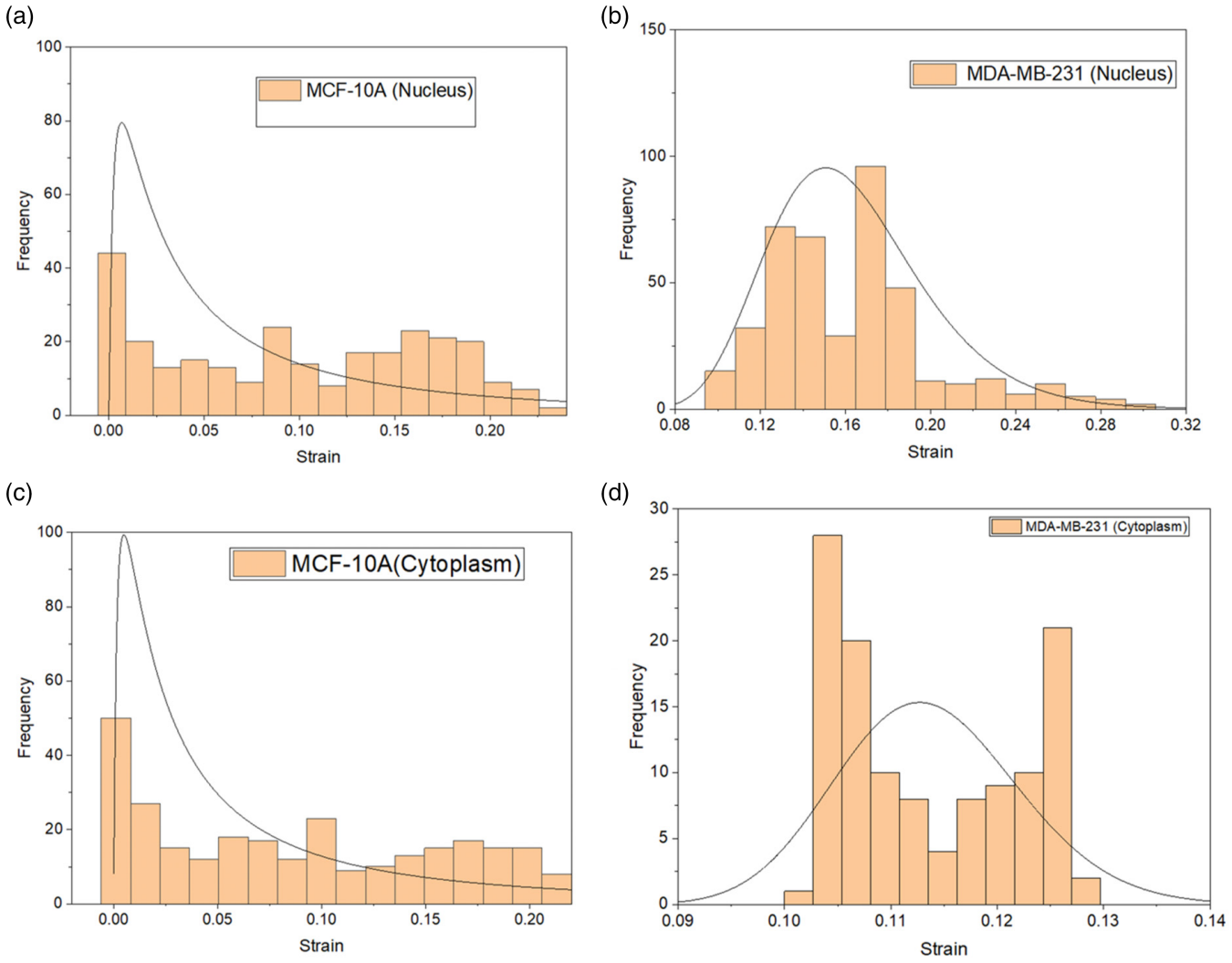


FIGURE 6 Frequency distribution at the onset of creep (Primary creep), for (A) the nucleus of the MCF-10A cell, (B) the nucleus of the MDA-MB-231, (C) cytoplasm of the MCF-10A, and (D) the cytoplasm of the MDA-MB-231

TABLE 3 Viscoelastic properties of normal and cancerous TNBC cells[25]

Cell type	Av. modulus, *E*, (Pa) nucleus	Av. modulus, *E* (Pa) cytoplasm	Av. viscosity, η (Pa s) nucleus	Av. viscosity, η (Pa s) cytoplasm	Av. relaxation time, τ (s) nucleus
MCF-10A	7966 ± 2536	3598 ± 1511	6868 ± 3095	3132 ± 1745	0.514 ± 0.290
MDA-MB-231	622 ± 399	261 ± 148	325 ± 234	215 ± 135	0.309 ± 0.353

Abbreviation: TNBC, triple-negative breast cancer.

were obtained at different stages of deformation. The evolution of strain under constant stress for both the normal and tumor cell resulted to creep. In Figure 4A–D, the difference in the strain evolution between the nucleus and cytoplasm of the normal MCF-10A cells and the tumorigenic MDA-MB-231 cells are shown at different creep stages.

Figure 4A,B show the initial creep stages of the cells for the nucleus and cytoplasm of both the normal and cancerous cells. At this stage, both types of cells, the normal and cancer cells exhibit fairly the same strain trends, where creep starts at a relatively rapid rate and slows with time. In this creep regime, the cells exhibit an instantaneous elastic phase before deformation, and their profiles are relatively similar, and thus their mechanical properties can be fairly compared. For the cancerous MDA-MB-231 cells, it was observed that they experienced more strain at shorter periods than the normal MCF-10A cells. Figure 4C,D show the secondary creep stage, and the strain during deformation of the structure of the cell. At this stage, the MDA-MB-231 cells experience a rather steady creep followed by

15524965, 2022, 5, Downloaded from https://onlinelibrary.wiley.com/doi/10.1002/jbm.a.37348 by Tsinghua University Library, Wiley Online Library on [05/11/2022]. See the Terms and Conditions (https://onlinelibrary.wiley.com/terms-and-conditions) on Wiley Online Library for rules of use; OA articles are governed by the applicable Creative Commons License

a sudden failure/detachment of the cell, in most cases, at the onset of the secondary creep stage, the MDA-MB-231 cells were fully deformed/detached from the substrate. For the normal MCF-10A cells, there is an increased resistance to deformation, giving rise to slower strain rates and increased strength. Most MCF-10A cells only experience failure or detachment, beyond the secondary creep stage (Tables 1 and 2).

The frequency distributions for the nucleus and cytoplasm for the normal MCF-10A and the tumorigenic MDA-MB-231 cells at the primary creep stage are shown in Figure 5A–D, while Figure 6A–D show the frequency distributions for the nucleus and cytoplasm for the normal MCF-10A and the tumorigenic MDA-MB-231 cells at the secondary creep regimes and the final stages of deformation. The shear strain data from the experiment was well characterized by lognormal distributions. The frequency distributions also revealed that the normal cells had a higher incidence of lower strain values, while the cancer cells had a higher incidence of larger strains. This was evident for both the nucleus and cytoplasm in the primary and secondary stages of creep in both the nucleus and cytoplasm of the normal (MCF-10A) and breast cancer (MDA-MB-231) cells.

3.2 | Cell viscoelastic properties

The viscoelastic properties of the non-tumorigenic and TNBC cells as described in our previous study,[25] were obtained using the three-element generalized Maxwell model (described in Section 2.6 of this article and shown schematically in Figure 3. From the strain-time analysis, the Maxwell model for viscoelastic materials was fitted to obtain Young's moduli, viscosities, and relaxation times for the different cell types. Hence, in this way, the spatial variations in the cell viscoelastic properties were characterized. The viscoelastic properties of the different cells, the non-tumorigenic breast, and tumorigenic cancer cells are presented in Table 3. It shows clear differences between the viscoelastic properties of the non-tumorigenic and TNBC cells. These variations in the cell viscoelastic properties could be due to the spatial variations in the cell cytoskeletal structures. Further investigations are therefore necessary for the validation of this claim. It is however seen from Table 3 that for the normal cells, the mechanical properties (Young's moduli and viscosities) were higher compared to the cancer cells. This variation in mechanical properties according to literature can be attributed to the role of the cytoskeleton on the cells.[25,27,28,31,32,41–43]

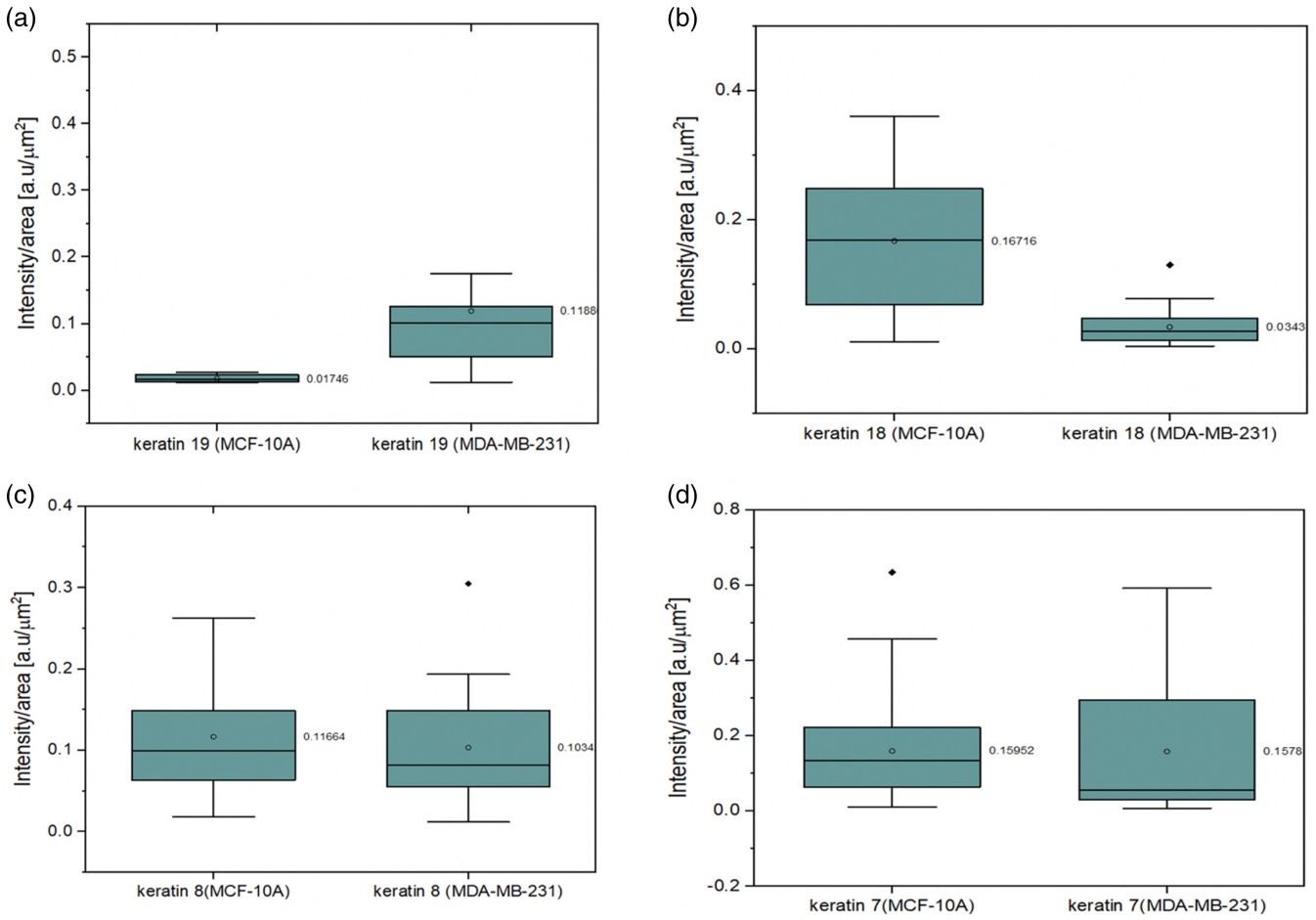


FIGURE 7 The fluorescence intensities/ area for the normal MCF-10A and cancerous MDA-MB-231 for the different proteins (A) keratin 19, (B) keratin 18, (C) keratin 8, (D) keratin 7, (E) vimentin, (F) tubulin, (G) actin

15524965, 2022, 5, Downloaded from https://onlinelibrary.wiley.com/doi/10.1002/jbm.a.37348 by Tsinghua University Library, Wiley Online Library on [05/11/2022]. See the Terms and Conditions (https://onlinelibrary.wiley.com/terms-and-conditions) on Wiley Online Library for rules of use; OA articles are governed by the applicable Creative Commons License

3.3 | Relative volume density distributions of the different proteins

The relative volume densities of the different cytoskeletal proteins were calculated by quantifying the average fluorescence intensities per unit area of a given protein and determining its relative volume densities as a function of the cell cytoskeletal proteins as seen in Equation (3).

$$\text{Relative volume density of A} = \frac{I_A}{I_n + I_A + I_B + I_C + ... + I_N}, \quad (3)$$

where I represent the average intensity/area of a given protein (volume of protein), n represents the nucleus of the cell, and A, B, C, N represent the different proteins of the cell. For each Z-stack image, the fluorescent intensity/area per Z-stack position/height was analyzed and their averages were computed. However, the expression of a certain amount of fluorescent intensity for a given protein represents the volume amount of that protein present in a particular cell per given area. After staining the cell with the required antibody reagent to reveal the amount of a particular protein, the cell was imaged under the confocal microscope to reveal the fluorescent intensities (volume amount of the protein) expressed by the cell. These intensities are then quantified using the Leica software, to determine the grayscale values per unit area.

The fluorescence intensities of the different cell proteins, the intermediate filaments (K7, K8, K18, K19, and vimentin), the microtubule (Tubulin), and the actin were analyzed, and their relative volume densities were determined. Figure 7 shows the average intensity per area of the different cytoskeletal proteins for the two types of cells (MCF-10A and MDA-MB-231). Numerically, for the fluorescence intensities, actin, keratin 18, keratin 8, and keratin 7 had higher intensities in the normal cells (MCF-10A) compared to the metastatic cells (MDA-MB-231). However, in the case of the metastatic cell line (MDA-MB-231), keratin 19, vimentin, and tubulin had higher fluorescence intensities, compared to that in the non-tumorigenic cells (MCF-10A). With a p-value of <.05, there were significant differences in the expression of keratin 19, keratin 18, vimentin, tubulin 8, and actin. There was no recorded statistical difference in the expression of keratin 7 and keratin 8 between the normal and the cancer cells.

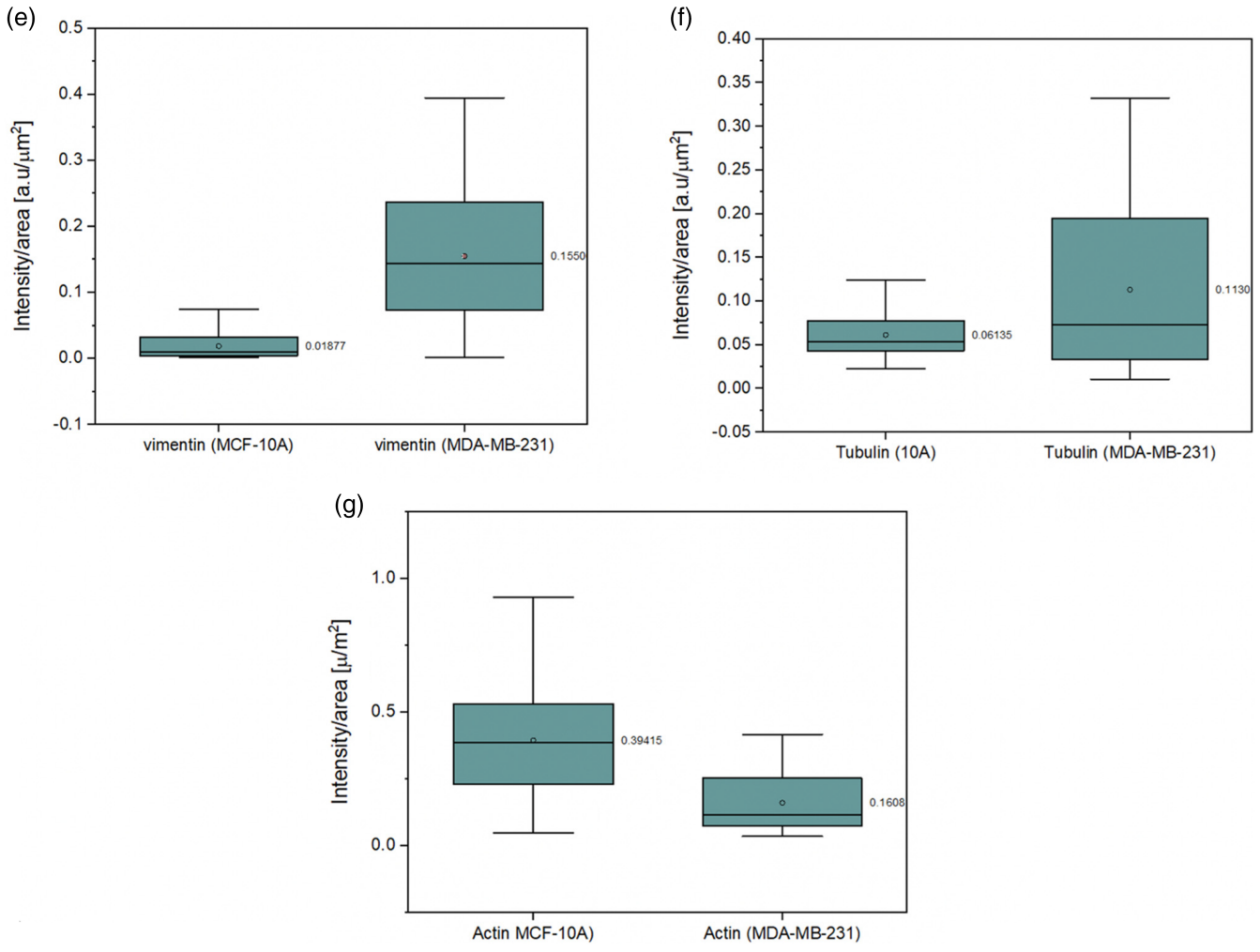


FIGURE 7 (Continued)

15524965, 2022, 5, Downloaded from https://onlinelibrary.wiley.com/doi/10.1002/jbm.a.37348 by Tsinghua University Library, Wiley Online Library on [05/11/2022]. See the Terms and Conditions (https://onlinelibrary.wiley.com/terms-and-conditions) on Wiley Online Library for rules of use; OA articles are governed by the applicable Creative Commons License

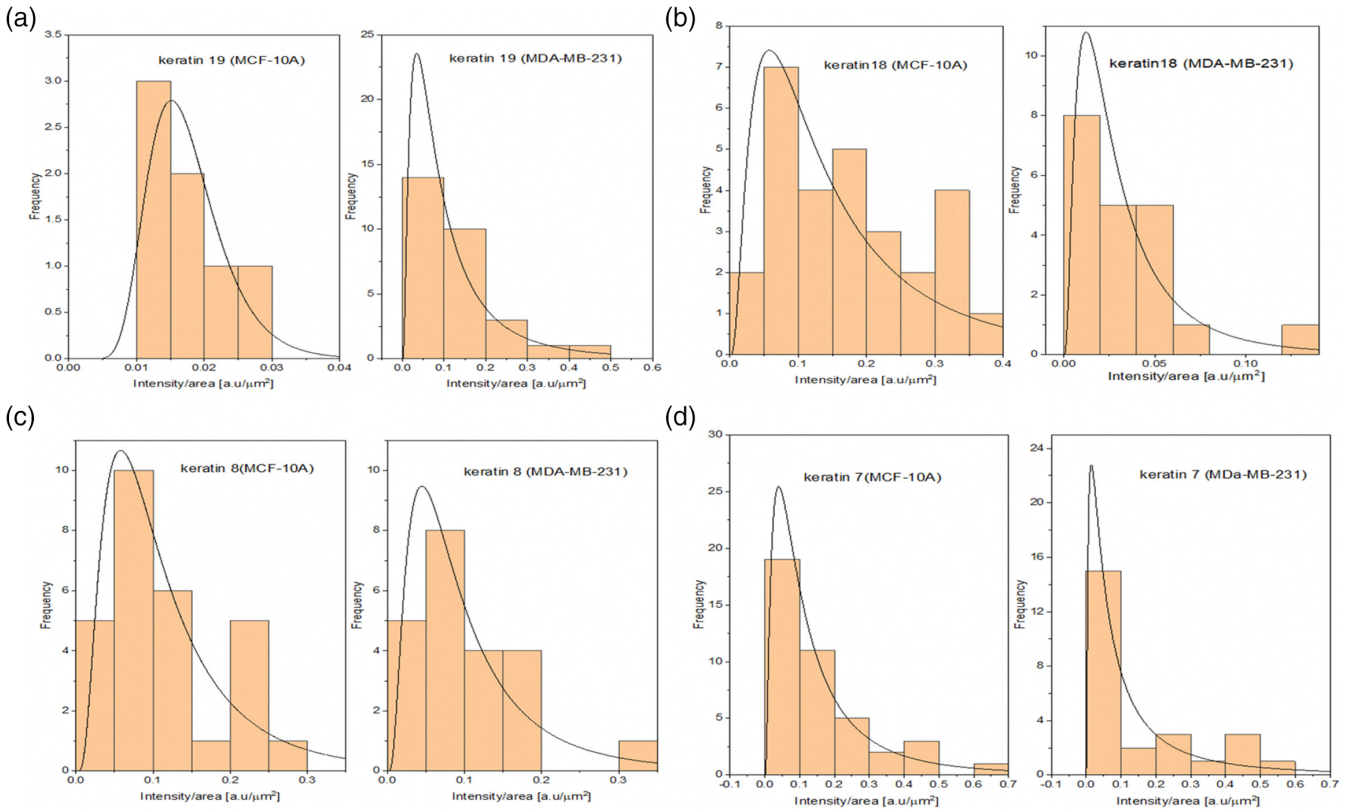


FIGURE 8 Frequency distribution of the different cytoskeleton proteins for the MCF-10A and MDA-MB-231 cells: (A) keratin 19, (B) keratin 18, (C) keratin 8, (D) vimentin, (E) tubulin, (F) actin

The frequency distribution curves in Figure 8 represent the probability density function for the expression of the different proteins. Most of the proteins were well characterized by a lognormal distribution, with a left skew in the distribution. Keratin 18, tubulin, and actin showed a more pronounced difference in distribution frequency and as such could be analyzed to give more insights as to how their cytoskeletal properties affect the mechanical strength of biological cells.

Figures 9 and 10 present the confocal images of the cell cytoskeletal proteins and the cell nucleus. These images show the variation in the volume of the proteins relative to one another across the two cell lines (MCF-10A) and (MDA-MB-231). The relative volume densities of each component of the cytoskeleton are calculated relative to the rest of the proteins and the nucleus. The nucleus and actin in both the non-tumorigenic MCF-10A cells and the cancerous MDA-MB-231 cells constitute the highest volumes relative to the rest of the cell constituents.

From the study, it was found that the nucleus and actin contain about 53% and 20%, respectively, of the total volume of the structure of the cell in the MCF-10A cell, and about 40% and 11%, respectively, of the total volume of the cell structure in the MDA-MB-231 cells, contributing largely to cell physiological and structural properties. Amongst the other cell proteins (IF and microtubulin), keratin 19, vimentin, and tubulin had the least volume densities relative to the other cell proteins in the MCF-10A cells. For the MDA-MB-231 cells, keratin 18 had the least volume percentages, with about 2% of the total volume. Keratin 19, keratin 8, and tubulin had 8.4%, 7.3%, and 8%, respectively, of the total protein volumes, while other IF proteins, such as vimentin and keratin 7, each had volume percentages of about 11%. While these percentages can be slightly different from one study to another, it gives a near approximation to the relative of amount of the different proteins in the cells as cancer progresses.

Figure 11A,B show further stained images of the actin substructures, the globular actin (G-actin), and the filamentous actin (F-actin). The F-actin stain reveals both the volume densities of both the filamentous, while the globular actin stain was stained using Alexa-594 DNaSe, and thus shows the individual structure for the G-actin.

The F-actin structure is found to express more at the base of the cell, away from the nucleus, and mostly at the boundaries between cells and between the surrounding cell environment. Its structures contain fibrous-like filaments, which have been found to create mechanical support to the cell. On the other hand, the globular actin is found to be more localized toward the nucleus of the cell and does not possess fibrous strands as the F-actin, but over time polymerizes to such filamentous actin structures. The filamentous actin structures in the normal cells are however seen mostly as bundles and are not expressed distinctly as single strands of filaments as in the MDA-MB-231 cells. Furthermore, the G-actin is seen to be expressed more in the cancerous cell than in normal cells. Table 4 shows the statistical variations of the relative volume densities of the cell cytoskeleton. It

15524965, 2022, 5, Downloaded from https://onlinelibrary.wiley.com/doi/10.1002/jbm.a.37348 by Tsinghua University Library, Wiley Online Library on [05/11/2022]. See the Terms and Conditions (https://onlinelibrary.wiley.com/terms-and-conditions) on Wiley Online Library for rules of use; OA articles are governed by the applicable Creative Commons License

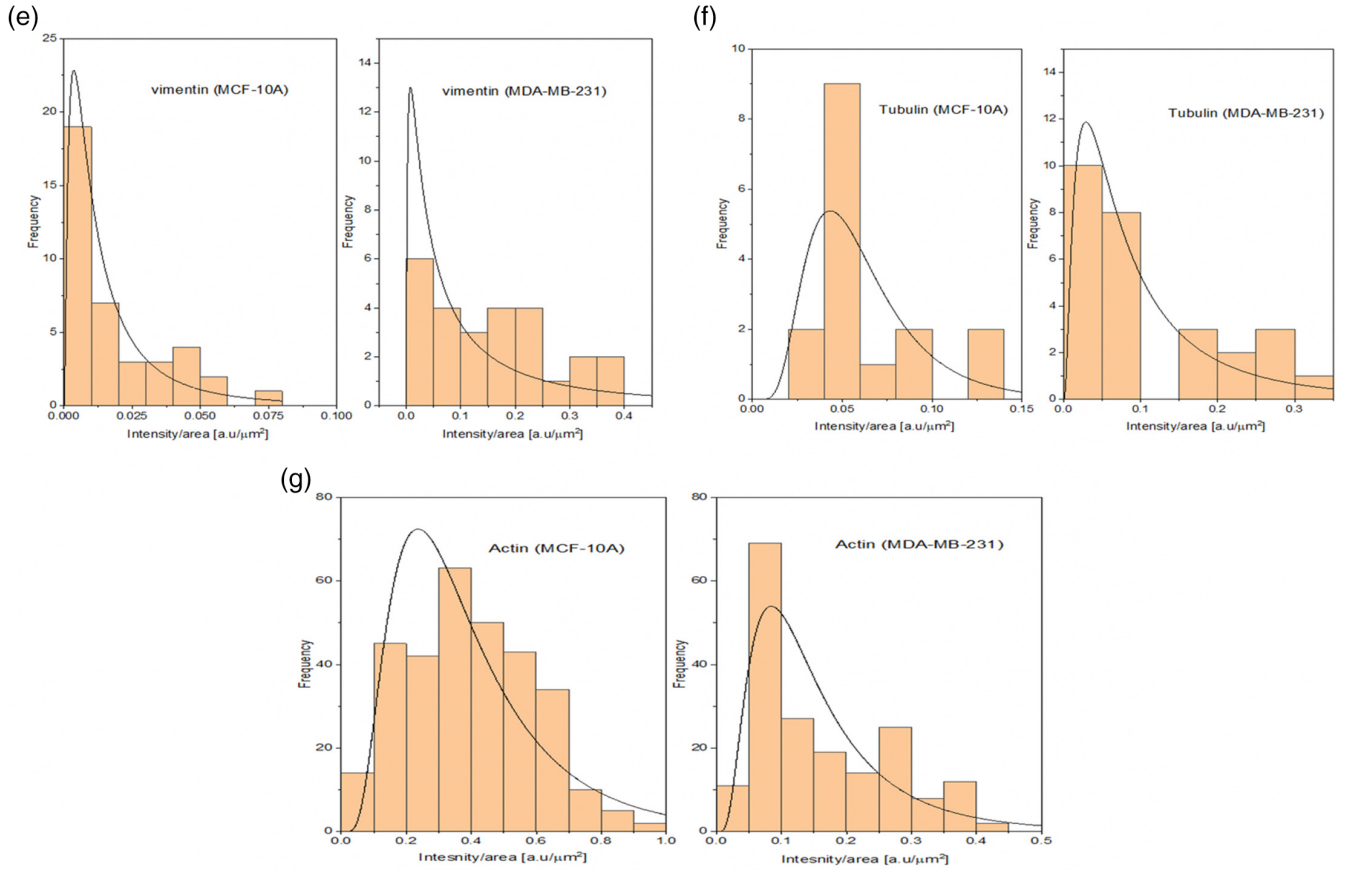


FIGURE 8 (Continued)

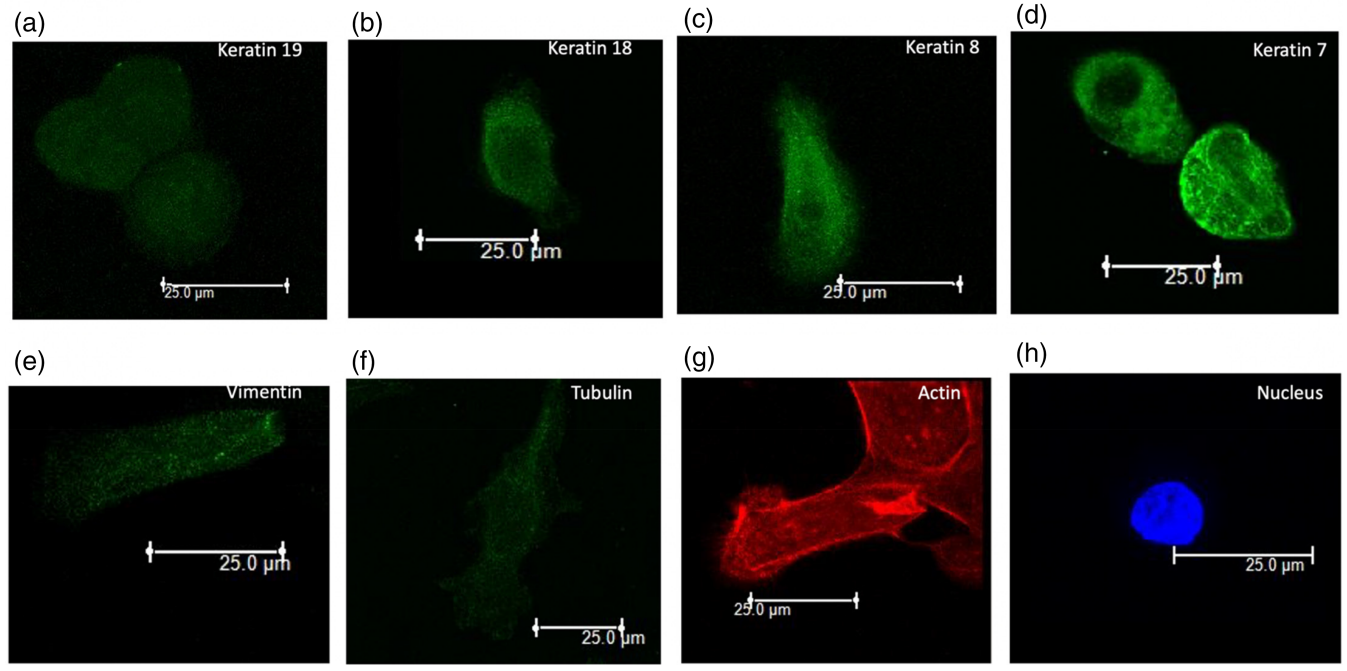


FIGURE 9 Confocal images of the cell cytoskeletal proteins and the nucleus for MCF-10A

15524965, 2022, 5, Downloaded from https://onlinelibrary.wiley.com/doi/10.1002/jbm.a.37348 by Tsinghua University Library, Wiley Online Library on [05/11/2022]. See the Terms and Conditions (https://onlinelibrary.wiley.com/terms-and-conditions) on Wiley Online Library for rules of use; OA articles are governed by the applicable Creative Commons License

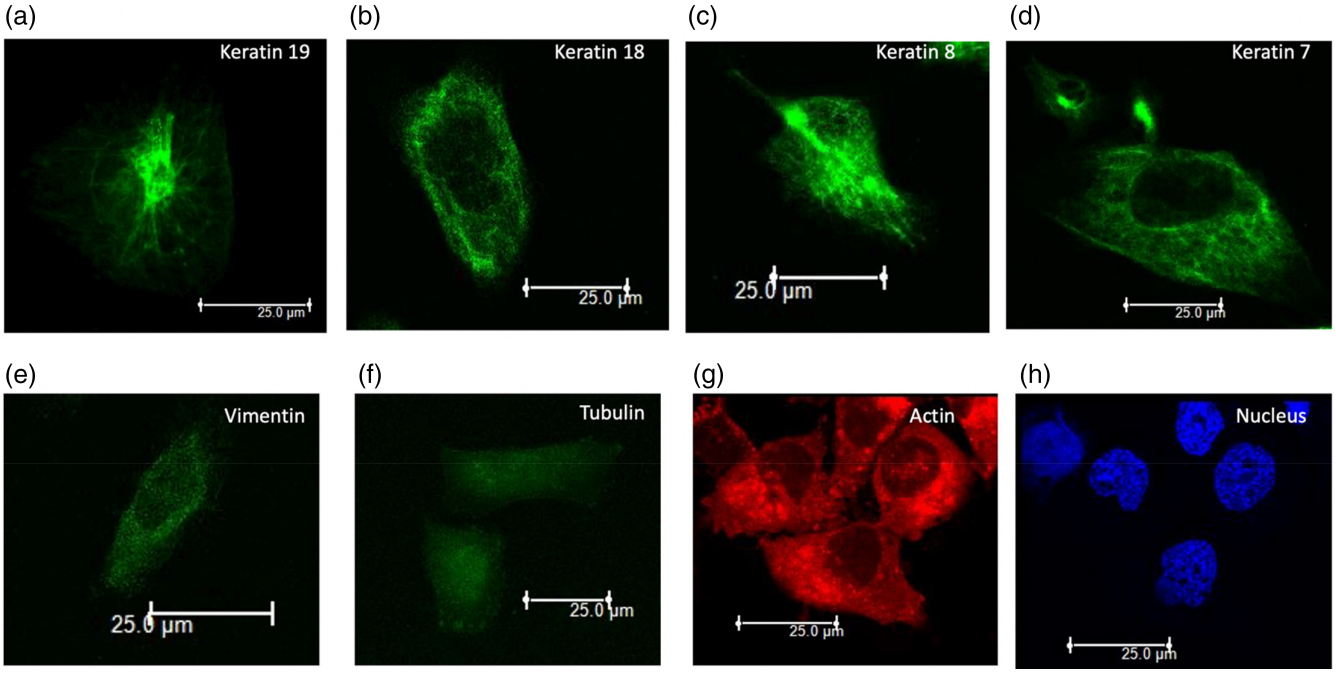


FIGURE 10 Confocal images of the cell cytoskeletal proteins and the nucleus for MDA-MB-231

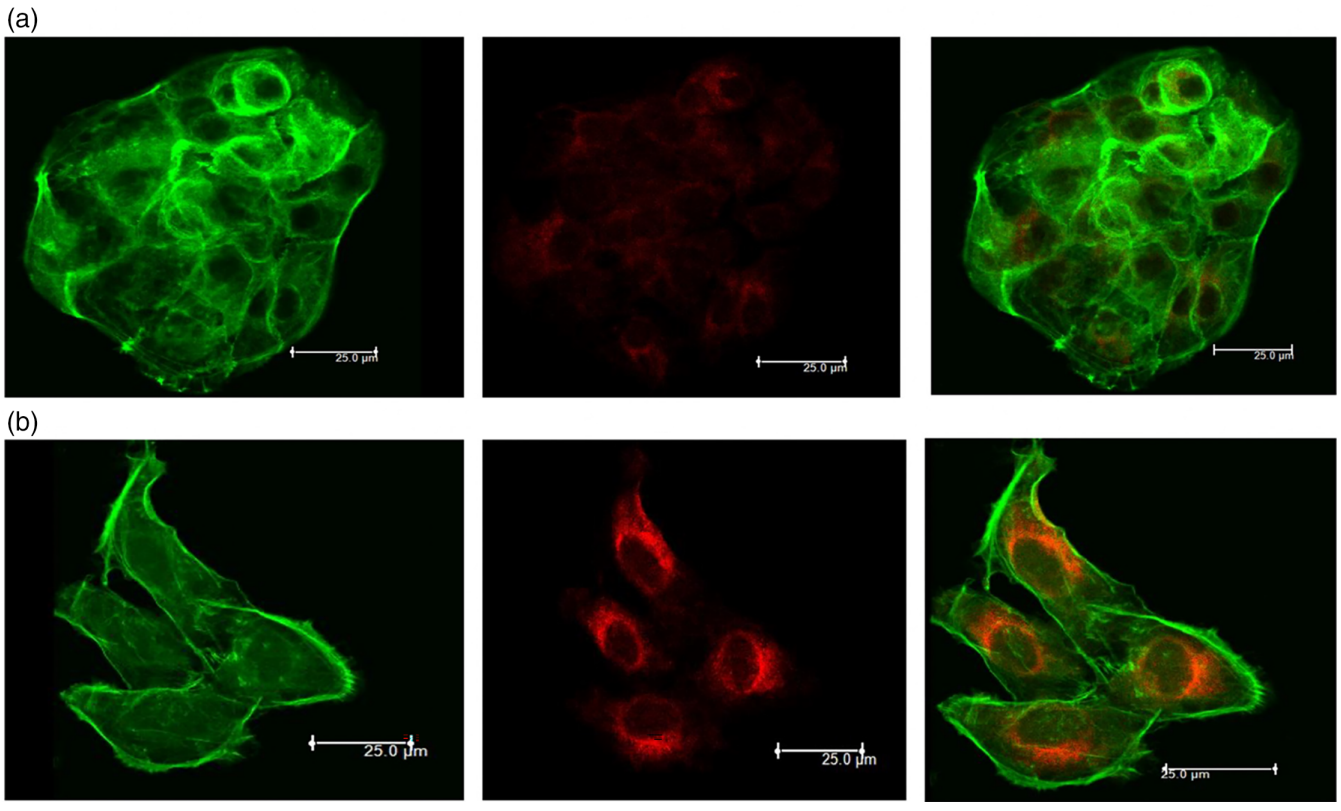


FIGURE 11 (A) Confocal images of the F-Actin and G -Actin structures for MCF-10A. (B) Confocal images of the F-Actin and G -Actin structures for MDA-MB-231

15524965, 2022, 5, Downloaded from https://onlinelibrary.wiley.com/doi/10.1002/jbm.a.37348 by Tsinghua University Library, Wiley Online Library on [05/11/2022]. See the Terms and Conditions (https://onlinelibrary.wiley.com/terms-and-conditions) on Wiley Online Library for rules of use; OA articles are governed by the applicable Creative Commons License

TABLE 4 The relative volume densities of the cell cytoskeleton

Protein	Relative volume density (MCF-10A)	Relative volume density (MDA-MB-231)	Tukey's sig value[a]	FPC mean Grouping (MCF-10A)[b]	FPC mean Grouping (MDA-MB-231)[b]	*p*-value[c]
Keratin 19	0.009	0.084	1	B	A	.021
Keratin 18	0.087	0.024	1	A	B	.000
Keratin 8	0.061	0.073	0	A	A	.507
Keratin 7	0.083	0.111	0	A	A	.965
Vimentin	0.010	0.110	1	B	A	.000
Tubulin	0.016	0.080	1	B	A	.049
Actin	0.205	0.114	1	A	B	.000
Nucleus	0.530	0.403	1	A	B	.000

[a]Means with Tukey's sig value =1, is significantly different.
[b]Means that do not share a letter are significantly different (Fisher pairwise comparisons [FPC]).
[c]Means with *p*-value <.05 are significantly different.

shows that statistically, keratin 19, keratin 18, vimentin, tubulin, actin, and cell nucleus are significantly different and thus their expression at different stages of tumor progression can be indicators of variabilities in cell states.

3.4 | Strain evolution analysis, the relative volume density of cell cytoskeletal structure, and correlation with cell mechanics

The relative volume density analyses of the cell cytoskeleton show that certain cell proteins are denser than others at different cell states are, and hence have a large role to play in the physical and mechanical structure of the cell. This attribute, however, contributes to the variation in the strain evolution of the cell during the deformation process. In the normal cell, there were more discrete-sized magnitudes of strain, resulting from short displacement spans. This, however, can be attributed to the denser actin structure of the normal cell, which provides mechanical structure and resists deformation, causing more discrete displacement of the structure and thus smaller strain values. This is, however, in line with results from several authors, where actin filaments were seen to provide robust mechanical structures and, degradation of actin caused a reduction in mechanical properties of the cell.[32,41,42,44]

In the cell cytoplasm and nucleus, the degree of strain was different. There was considerably more strain in the cell cytoplasm than there are in the cell nucleus during the initial stages of creep, but with constant stress, the nucleus experienced considerable higher strain than the cytoplasm, where the proteins in the cytoplasm re-organize to withstand stress, thereby causing lesser deformation and strain. This, however, could be attributed to the internal structure of the cell, whereby the cell nucleus is a homogeneous structure, with relatively lesser structural ability to withstand stress than the layered cytoplasm, which consists of heterogeneously different components that can reduce the ability of the cell to undergo deformation.

The microstructure of the cell shows a higher density of actin and keratin 18 in the normal MCF-10A cells, and a higher density of the other proteins (Keratin 19, keratin 7, keratin 8, vimentin, and tubulin) in the cancerous MDA-MB-231 cells. This variation in the expression of the proteins is interesting in the understanding of the specific role of some of the proteins in cancer progression. The relative volume density of the actin microfilament and keratin 18 suggests that for the normal cells, these proteins help to provide considerable resistance to applied stress. The denser these proteins, the more mechanical strength it possesses to withstand stress.

In this study, it was observed that the actin filament contributes largely to the total volume of the cell structure, with the total cell cytoskeletal microstructure made up of about 20% actin in the normal cell and about 11% in the cancerous cells, and as such plays, a key role in cell shape and movement, providing mechanical structure and motility.[45] Therefore, the density of the actin filament can be said to largely contribute to the variation in the mechanical structure of the cell. Over-expression of other proteins such as vimentin, tubulin, keratin 19, keratin 7, and keratin 8 can be correlated to the decreased mechanical properties of the cancerous MDA-MB-231. Most IF proteins such as keratins have been linked to low bending stiffness and decreased mechanical properties of cells.[46]

4 | DISCUSSION

The results of the current study are useful in the characterization of the structure and properties of the normal breast cells (MCF-10A) and the metastatic TNBC cells. First, the results show that the fluorescence images with the mechanical properties of the cells provide important information that can be used to describe the cell structure

15524965, 2022, 5, Downloaded from https://onlinelibrary.wiley.com/doi/10.1002/jbm.a.37348 by Tsinghua University Library, Wiley Online Library on [05/11/2022]. See the Terms and Conditions (https://onlinelibrary.wiley.com/terms-and-conditions) on Wiley Online Library for rules of use; OA articles are governed by the applicable Creative Commons License

in ways that can discriminate between non-tumorigenic cells and tumorigenic cells. Such digital imaging could enable the identification of TNBC cells in future biopsies. However, further work is needed to determine the extent to which fluorescence imaging techniques can be used to discriminate between cancer cells at different stages of tumor progression.

The current work also identifies significant differences between the components of the cytoskeletal structures in non-tumorigenic cells and tumorigenic cells. Hence, beyond the decrease in the actin cytoskeletal structural components that occur with cancer progression, the current work suggests that variations in microtubulin and keratin components can also occur in ways that can be used to distinguish between non-tumorigenic and tumorigenic states and correlate them with the individual mechanical properties of the cell. Further work is needed to establish the extent to which the identification of these structural components can be used to diagnose the onset and progression of breast cancer under clinical scenarios.

Finally, it is of interest to note that the above changes in the cytoskeletal structures can be correlated to the creep strain rates and viscoelastic properties, which we have shown to change significantly, as the cells evolve from non-tumorigenic to tumorigenic states.[13] In particular, the dependence of the stiffness and viscosity (of the nuclei and cytoplasm) appear to provide strong indications of the presence of TNBC. The trends in the cell viscoelastic properties can also be correlated with changes in cell cytoskeletal proteins in ways that could inform future analyses of cell biopsies and the use of shear assay techniques for the determination of mechanical biomarkers for the detection of TNBC in biopsies. Future work is, therefore, needed in the clear-cut understanding of how the expression of these proteins affects cell mechanics and promotes tumor progression. Cytoskeletal inhibitors can, also, be used for further studies of their individual effects on the cell. Finally, shear assay techniques can be used to m study of the physiological responses of cells under controlled shear/laminar flow conditions. These are clearly opportunities for future work.

5 | CONCLUSION

In this study, we analyzed the variations in the mechanical properties and cytoskeletal proteins of the tumorigenic TNBC cells and non-tumorigenic breast cells. We hoverer concluded from the study, that the shear assay measurements of cell viscoelastic properties (Young's moduli and viscosities of the nuclei and cytoplasm) reveal significant differences between the viscoelastic properties of the non-tumorigenic MCF-10A cells and those of the tumorigenic MDA-MB-231 cells. The difference in their means and error deviations statistically proves that a significant difference exists between the properties of the normal cells and the cancerous cells. The results suggest that Young's moduli and viscosities of the nuclei and the cytoplasm may be used to distinguish between non-tumorigenic breast cells and tumorigenic TNBC cells. Creep strain rates were faster in the cancerous MDA-MB-231 cells compared to those in the normal MCF-10A cells. There were also higher strains in the nucleus of both the normal MCF-10A cells and cancerous MDA-MB-231 cells than in the cytoplasm of the cells. The internal structure of the heterogeneous cytoplasm gives it more rigidity enough to withstand applied stress, than the nucleus.

The fluorescence intensities of the different components of the cell cytoskeletal structure (actin microfilaments, microtubules, and intermediate filaments) can be used to determine the relative volume densities of the individual components of the cell cytoskeletal structure, and hence can be used to distinguish between the structures of non-tumorigenic MCF-10A and tumorigenic MDA-MB-231 TNBC cells. The relative volume density of the intermediate filaments (keratin 19, keratin 18, keratin 8, keratin 7, and vimentin), and microtubules (tubulin) are different in non-tumorigenic breast cells and tumorigenic TNBC cells. In addition, the relative volume densities of the intermediate filaments are higher in the metastatic MDA-MB-231 TNBC cells. For keratin 18 and actin, their relative volume densities were greater in the non-tumorigenic (MCF-10A cells) than in the metastatic MDA-MB-231 cells. Similar trends are observed for the microtubules, for which the expression of the tubulin is greater in the metastatic MDA-MB-231 cells than in non-tumorigenic MCF-10A cells.

There were statistical differences in the relative volume density of some proteins such as keratin 19, keratin 18, tubulin, vimentin, and actin. However, no significant differences were obtained for keratin 8, and keratin 7. The strains of the nucleus and cytoplasm between the normal MCF-10A and MDA-MB-231 cells had significant differences both at the elastic deformation stage (primary regime) and plastic deformation (tertiary regime).

A combination of the relative volume densities and shear assay measurements can be used to provide diagnostic insights for the characterization of non-tumorigenic and tumorigenic TNBC cells. Such approach can be enabled by fluorescence microscopy imaging (to reveal the incidence and relative volume densities of the cytoskeletal proteins, especially actin) and shear assay measurements of creep strain rates/cell viscoelastic properties (Young's moduli/viscosities of the nuclei and cytoplasm). These can be used, respectively, as fluorescence and mechanical biomarkers, for the classification of breast cells into non-tumorigenic breast cells and tumorigenic TNBC cells.

Lognormal distributions were used to characterize the fluorescence intensities and strain rates of the different cells, while for the characterization of the viscoelastic properties of the cell, the normal distribution provided the best fit. These distributions are best for the determination of the geometric means and variations in the statistical data of the cell properties.

ACKNOWLEDGMENTS

The authors are also grateful to the African University of Science and Technology, Abuja, and Worcester Polytechnic Institute for the material and financial support of the work.

CONFLICT OF INTEREST

The authors declare no potential conflict of interest.

15524965, 2022, 5, Downloaded from https://onlinelibrary.wiley.com/doi/10.1002/jbm.a.37348 by Tsinghua University Library, Wiley Online Library on [05/11/2022]. See the Terms and Conditions (https://onlinelibrary.wiley.com/terms-and-conditions) on Wiley Online Library for rules of use; OA articles are governed by the applicable Creative Commons License

DATA AVAILABILITY STATEMENT

The data that support the findings of this study are available on request from the corresponding author. The data are not publicly available due to privacy restrictions.

REFERENCES

1. Al-Azri MH. Delay in cancer diagnosis: causes and possible solutions. *Oman Med J*. 2016;31(5):325-326. doi:10.5001/omj.2016.65
2. Chakraborty S, Rahman T. The difficulties in cancer treatment. *Ecancermedicalscience*. 2012;6:ed16. doi:10.3332/ecancer.2012.ed16
3. Azamjah N, Soltan-Zadeh Y, Zayeri F. Global trend of breast cancer mortality rate: a 25-year study. *Asian Pac J Cancer Prev*. 2019;20(7):2015-2020. doi:10.31557/APJCP.2019.20.7.2015
4. Collignon J, Lousberg L, Schroeder H, Jerusalem G. Triple-negative breast cancer: treatment challenges and solutions. *Breast Cancer*. 2016;8:93-107. doi:10.2147/BCTT.S69488
5. Melzer C, von der Ohe J, Hass R. Breast carcinoma: from initial tumor cell detachment to settlement at secondary sites. *Biomed Res Int*. 2017;2017:1-11. doi:10.1155/2017/8534371
6. Abulkhair O, Moghraby JS, Badri M, Alkushi A. Clinicopathologic features and prognosis of triple-negative breast cancer in patients 40 years of age and younger in Saudi Arabia. *Hematol Oncol Stem Cell Ther*. 2012;5(2):101-106. doi:10.5144/1658-3876.2012.101
7. Stovgaard ES, Nielsen D, Hogdall E, Balslev E. Triple negative breast cancer–prognostic role of immune-related factors: a systematic review. *Acta Oncol*. 2018;57(1):74-82. doi:10.1080/0284186X.2017.1400180
8. Ovcaricek T, Frkovic SG, Matos E, Mozina B, Borstnar S. Triple negative breast cancer - prognostic factors and survival. *Radiol Oncol*. 2011;45(1):46-52. doi:10.2478/v10019-010-0054-4
9. Yin L, Duan JJ, Bian XW, Yu SC. Triple-negative breast cancer molecular subtyping and treatment progress. *Breast Cancer Res*. 2020;22(1):61. doi:10.1186/s13058-020-01296-5
10. Reddy SM, Barcenas CH, Sinha AK, et al. Long-term survival outcomes of triple-receptor negative breast cancer survivors who are disease free at 5 years and relationship with low hormone receptor positivity. *Br J Cancer*. 2018;118(1):17-23. doi:10.1038/bjc.2017.379
11. Gonçalves H, Guerra MR, Duarte Cintra JR, Fayer VA, Brum IV, Bustamante Teixeira MT. Survival study of triple-negative and non–triple-negative breast cancer in a Brazilian cohort. *Clin Med Insights Oncol*. 2018;12:1179554918790563. doi:10.1177/1179554918790563
12. Li QS, Lee GYH, Ong CN, Lim CT. AFM indentation study of breast cancer cells. *Biochem Biophys Res Commun*. 2008;374(4):609-613. doi:10.1016/j.bbrc.2008.07.078
13. Cai X, Xing X, Cai J, Chen Q, Wu S, Huang F. Connection between biomechanics and cytoskeleton structure of lymphocyte and Jurkat cells: an AFM study. *Micron*. 2010;41(3):257-262. doi:10.1016/j.micron.2009.08.011
14. Lee LM, Liu AP. The application of micropipette aspiration in molecular mechanics of single cells. *J Nanotechnol Eng Med*. 2014;5(4):0408011-0408016. doi:10.1115/1.4029936
15. Li YJ, Zhang HJ, Xue CD, et al. A microfluidic micropipette aspiration device to study single-cell mechanics inspired by the principle of Wheatstone bridge. *Micromachines*. 2019;10(2):131. doi:10.3390/mi10020131
16. Zhang H, Liu KK. Optical tweezers for single cells. *J R Soc Interface*. 2008;5(24):671-690. doi:10.1098/rsif.2008.0052
17. Kumar S, Weaver VM. Mechanics, malignancy, and metastasis: the force journey of a tumor cell. *Cancer Metastasis Rev*. 2009;28(1-2):113-127. doi:10.1007/s10555-008-9173-4
18. Vanapalli SA, Duits MHG, Mugele F. Microfluidics as a functional tool for cell mechanics. *Biomicrofluidics*. 2009;3(1):3-5. doi:10.1063/1.3067820
19. Takahashi R, Kuribayashi-Shigetomi K, Tsuchiya M, Subagyo A, Sueoka K, Okajima T. High-throughput measurements of cell mechanics using atomic force microscopy with micro-patterned substrates. Paper presented at: 2013 International Symposium on Micro-NanoMechatronics and Human Science, MHS 2013; 2013, pp. 7–9. doi: 10.1109/MHS.2013.6710471
20. Wei M-T, Zaorski A, Yalcin HC, et al. A comparative study of living cell micromechanical properties by oscillatory optical tweezers. *Opt Express*. 2008;16(12):8594-8603. doi:10.1364/oe.16.008594
21. Ravetto A, Anderson PDA, Bouten CVC, den Toonder JMJ. Microfluidics for single cell mechanical characterization: a review. *SM J Biomed Bioeng*. 2017;3(2):1016.
22. Guillou L, Dahl JB, Lin JMG, et al. Measuring cell viscoelastic properties using a microfluidic extensional flow device. *Biophys J*. 2016;111(9):2039-2050. doi:10.1016/j.bpj.2016.09.034
23. Ani CJ, Obayemi JD, Uzonwanne VO, et al. A shear assay study of single Normal/breast cancer cell deformation and detachment from poly-Di-methyl-Siloxane (PDMS) surfaces. *J Mech Behav Biomed Mater*. 2019;91:76-90. doi:10.1016/j.jmbbm.2018.11.012
24. Onwudiwe K, Hu J, Obayemi J, et al. Actin cytoskeletal structure and the statistical variations of the mechanical properties of non-tumorigenic breast and triple-negative breast cancer cells. *J Mech Behav Biomed Mater*. 2021;119:104505. doi:10.1016/j.jmbbm.2021.104505
25. Hu J, Zhou Y, Obayemi JD, Du J, Soboyejo WO. An investigation of the viscoelastic properties and the Actin cytoskeletal structure of triple negative breast cancer cells. *J Mech Behav Biomed Mater*. 2018;86:1-13. doi:10.1016/j.jmbbm.2018.05.038
26. Cao Y, Bly R, Moore W, Gao Z, Cuitino AM, Soboyejo W. Investigation of the viscoelasticity of human osteosarcoma cells using a shear assay method. *J Mater Res*. 2006;21(8):1922-1930. doi:10.1557/jmr.2006.0235
27. Fletcher DA, Mullins RD. Cell mechanics and the cytoskeleton. *Nature*. 2010;463(7280):485-492. doi:10.1038/nature08908
28. Pegoraro AF, Janmey P, Weitz DA. Mechanical properties of the cytoskeleton and cells. *Cold Spring Harb Perspect Biol*. 2017;9(11):a022038. doi:10.1101/cshperspect.a022038
29. Grady ME, Composto RJ, Eckmann DM. Cell elasticity with altered cytoskeletal architectures across multiple cell types. *J Mech Behav Biomed Mater*. 2016;61:197-207. doi:10.1016/j.jmbbm.2016.01.022
30. Ketene AN, Schmelz EM, Roberts PC, Agah M. The effects of cancer progression on the viscoelasticity of ovarian cell cytoskeleton structures. *Nanomedicine*. 2012;8(1):93-102. doi:10.1016/j.nano.2011.05.012
31. Tabatabaei M, Tafazzoli-Shadpour M, Khani MM. Correlation of the cell mechanical behavior and quantified cytoskeletal parameters in normal and cancerous breast cell lines. *Biorheology*. 2019;56(4):207-219. doi:10.3233/BIR-190214
32. Ghaffari H, Saidi MS, Firoozabadi B. Biomechanical analysis of Actin cytoskeleton function based on a spring network cell model. *Proc Inst Mech Eng C J Mech Eng Sci*. 2017;231(7):1308-1323. doi:10.1177/0954406216668546
33. Etienne-Manneville S. Actin and microtubules in cell motility: which one is in control? *Traffic*. 2004;5(7):470-477. doi:10.1111/j.1600-0854.2004.00196.x
34. Fuchs E, Cleveland DW. A structural scaffolding of intermediate filaments in health and disease. *Science*. 1998;279(5350):514-519. doi:10.1126/science.279.5350.514
35. Sun BO, Fang Y, Li Z, Chen Z, Xiang J. Role of cellular cytoskeleton in epithelial-mesenchymal transition process during cancer progression. *Biomed Rep*. 2015;3:603-610. doi:10.3892/br.2015.494
36. Sant GR, Knopf KB, Albala DM. Live-single-cell phenotypic cancer biomarkers-future role in precision oncology ? *npj Precis Oncol*. 2017;1:1-6. doi:10.1038/s41698-017-0025-y
37. Klingler-Hoffmann M, Mittal P, Hoffmann P. The emerging role of cytoskeletal proteins as reliable biomarkers. *Proteomics*. 2019;19(21-22):e1800483. doi:10.1002/pmic.201800483

15524965, 2022, 5, Downloaded from https://onlinelibrary.wiley.com/doi/10.1002/jbm.a.37348 by Tsinghua University Library, Wiley Online Library on [05/11/2022]. See the Terms and Conditions (https://onlinelibrary.wiley.com/terms-and-conditions) on Wiley Online Library for rules of use; OA articles are governed by the applicable Creative Commons License

38. Burgess A, Vigneron S, Brioudes E, Labbé JC, Lorca T, Castro A. Loss of human Greatwall results in G2 arrest and multiple mitotic defects due to deregulation of the cyclin B-Cdc2/PP2A balance. *Proc Natl Acad Sci U S A*. 2010;107(28):12564-12569. doi:10.1073/pnas.0914191107
39. Gavet O, Pines J. Progressive activation of CyclinB1-Cdk1 coordinates entry to mitosis. *Dev Cell*. 2010;18(4):533-543. doi:10.1016/j.devcel.2010.02.013
40. Cao Y, Bly R, Moore W, Gao Z, Cuitino AM, Soboyejo W. On the measurement of human osteosarcoma cell elastic modulus using shear assay experiments. *J Mater Sci Mater Med*. 2007;18(1):103-109. doi:10.1007/s10856-006-0667-8
41. Moreno-Flores S, Benitez R, Vivanco MDM, Toca-Herrera JL. Stress relaxation and creep on living cells with the atomic force microscope: a means to calculate elastic moduli and viscosities of cell components. *Nanotechnology*. 2010;21(44):445101. doi:10.1088/0957-4484/21/44/445101
42. Brückner BR, Nöding H, Skamrahl M, Janshoff A. Mechanical and morphological response of confluent epithelial cell layers to reinforcement and dissolution of the F-Actin cytoskeleton. *Prog Biophys Mol Biol*. 2019;144:77-90. doi:10.1016/j.pbiomolbio.2018.08.010
43. Zhang X, Pei Z, Ji C, Zhang X, Xu J, Wang J. Novel insights into the role of the cytoskeleton in cancer. *Cytoskeleton: Struct Dyn Funct Dis*. 2017. doi:10.5772/66860
44. Kubitschke H, Schnauss J, Nnetu KD, Warmt E, Stange R, Kaes J. Actin and microtubule networks contribute differently to cell response for small and large strains. *New J Phys*. 2017;19(9):093003. doi:10.1088/1367-2630/aa7658.
45. Pollard TD, Cooper JA. Actin, a central player in cell shape and movement. *Science*. 2009;326(5957):1208-1212. doi:10.1126/science.1175862
46. Ramms L, Fabris G, Windoffer R, et al. Keratins as the main component for the mechanical integrity of keratinocytes. *Proc Natl Acad Sci U S A*. 2013;110(46):18513-18518. doi:10.1073/pnas.1313491110

How to cite this article: Onwudiwe K, Obayemi J, Hu J, et al. Investigation of creep properties and the cytoskeletal structures of non-tumorigenic breast cells and triple-negative breast cancer cells. *J Biomed Mater Res*. 2022;110(5):1004-1020. doi:10.1002/jbm.a.37348

15524965, 2022, 5, Downloaded from https://onlinelibrary.wiley.com/doi/10.1002/jbm.a.37348 by Tsinghua University Library, Wiley Online Library on [05/11/2022]. See the Terms and Conditions (https://onlinelibrary.wiley.com/terms-and-conditions) on Wiley Online Library for rules of use; OA articles are governed by the applicable Creative Commons License